
CHALMERS
UNIVERSITY OF TECHNOLOGY

# Modelling of Articulated Heavy Vehicles for Computation of Accurate Safe Operating Envelope for Yaw Stability

# MODELLING OF ARTICULATED HEAVY VEHICLES FOR COMPUTATION OF ACCURATE SAFE OPERATING ENVELOPE FOR YAW STABILITY

| U. ERDINC | M. JONASSON | M. SADEGHI KATI | B. JACOBSON | J. FREDRIKSSON | L. LAINE |
|---|---|---|---|---|---|
| Industrial PhD student employed by Volvo Group Trucks Technology and performing studies at Chalmers University of Technology. | Senior researcher at Chalmers University of Technology. Obtained PhD from KTH Royal University of Technology. | Lead control system engineer at Volvo Group Trucks Technology. Obtained PhD from Chalmers University of Technology. | Professor at Chalmers University of Technology. Obtained PhD from Chalmers University of Technology. | Professor at Chalmers University of Technology. Obtained PhD from Chalmers University of Technology. | Innovation and research strategist at Volvo Group Trucks Technology and adjunct professor at Chalmers University of Technology. Obtained PhD from Chalmers University of Technology. |

## Abstract

As articulated heavy vehicles switch to electric power, new ways of allocating wheel forces have emerged. To improve energy efficiency, it is increasingly common to use propulsion or regenerative braking on only one unit of the vehicle combination. This leads to yaw stability problems, mainly jackknifing if the towing unit has excessive wheel forces, or trailer swing if the trailing unit has excessive wheel forces. Hence, it becomes important to allocate the total force request into different units and actuators in a safe way.

This paper formulates a nonlinear two-track model with a nonlinear tire model, combined slip, and roll degree of freedom. Thus, the presented model can accurately simulate brake-in-turn and propel-in-turn maneuvers at high lateral accelerations. And it can be used to study when the yaw instability occurs and understand if the maneuver is safe or not.

One way to ensure safe control allocation is by implementing a safe operating envelope that restricts the allocation within predefined limits. This helps maintain control of the system and prevent any potential safety hazards. In this paper, a nonlinear two-track model is utilized to simulate a range of lateral accelerations and various combinations of braking forces between the tractor and semitrailer. Through this process, an envelope is obtained which is then compared to an envelope generated from a single-track model and validated against high-fidelity model-based envelopes. This rigorous process helps to ensure the accuracy and reliability of the two-track model.

**Keywords:** Yaw Instability, Jackknifing, Trailer Swing, Combination Spin-out, Articulated Heavy Vehicle, Electric Vehicle, Safe Operating Envelope

## 1. Introduction

Articulated heavy vehicles (AHVs), which consist of multiple units joined via articulated points, play an essential role in fulfilling transport missions by transporting large volumes of cargo. Owing to the recent developments in electrified vehicles, not only the leading units (tractors) of the AHVs, but also the trailing units (trailers and dollies) have potential to be electrified. Although this method of transportation would undoubtedly be more energy-efficient, it also raises safety concerns such as jackknifing and trailer swing. If a large amount of propulsion or brake force is applied at the leading unit, jackknifing may occur. Conversely, if a large amount of propulsion or brake force is applied at the trailing unit, trailer swing may occur. In the distributed control of multi-unit vehicles, it is crucial to maintain power and energy efficiency while also being mindful of the forces being requested by the controllers per unit. Excessive brake or propulsion forces per unit can lead to yaw stability issues, which can compromise the overall control and performance of the vehicles.

Safe operating envelopes (SOEs) are widely used and studied in various industries, including aircrafts (Van Oort et al., 2011; Lombaerts et al., 2015; Lombaerts et al., 2013; Zhang et al., 2016), submarines (Park et al., 2018), and nuclear plants (Prime et al., 2008). In automotive engineering, SOE refers to the range of input values or states in which a vehicle can operate safely and effectively, see Brown et al., 2017; Cui et al., 2021; Bobier et al., 2013; Bobier et al., 2010; Beal et al., 2011. However, these studies are mostly limited to single-unit vehicles. They are mainly taking side-slip angles and yaw rates into account, and not considering the actuator inputs. Hansson et al. (2022), on the other hand, defined an SOE for a multi-unit vehicle, mainly for electric trailer propulsion. Erdinc et al. (2023a; 2023b) defined the SOE based on the force generated by the actuators (electric motor forces and brake forces per each unit) and as a function of the normalized lateral acceleration (normalized with respect to the friction) for the AHVs. By utilizing the SOE, a motion controller can prevent requesting unsafe combinations of actuator forces per unit, thereby ensures safety. SOE can be used as inequality constraints with an energy-efficient controller, such as the power loss minimization algorithm presented by Janardhanan et al. (2022), to ensure the best energy efficiency while keeping the vehicle safe and ensuring an unsafe combination of actuator forces are not requested.

According to Erdinc et al. (2023a), a nonlinear single-track model that incorporates a saturated tire model can be utilized to simulate various combinations of braking and propulsion for tractor and semitrailer under varying lateral accelerations. By utilizing a safety assessment criterion that is based on the deviations in the side-slip angle of the individual units, it is possible to classify each simulation as either safe or unsafe. The combinations of safe maneuvers identified through this process can be used to establish the SOE for the vehicle combination.

Erdinc et al. (2023b) showed that a high-fidelity simulation model called “Volvo Transport Model” (VTM) can also be used to obtain the SOE. In addition, they validated the accuracy of the SOE obtained through VTM by comparing it with results from real vehicle tests.

Single-track model (Erdinc et al., 2023a) has low accuracy for higher lateral accelerations as it is missing lateral load transfer. In this paper, first, a two-track model is proposed. This model is simulated for various lateral accelerations and different combinations of tractor and semitrailer braking forces. Then, by using safety criteria based on side slip angle deviations of the units, all maneuvers are classified as safe and unsafe. The envelope that covers the safe maneuvers is named as “safe operating envelope” (SOE). The SOE obtained with the proposed two-track model is then compared with the SOEs obtained with the single-track model (Erdinc et al., 2023a) and VTM high-fidelity model (Erdinc et al., 2023b). Reasons for the differences and the accuracy of the models are discussed.

## 2. Non-linear Two-Track Model for Tractor-Semitrailer Combination

A non-linear two-track model for articulated heavy vehicles can be obtained by considering the following set of free-body diagrams. Any possible rear axle group of the tractor and semitrailer axle group are assumed to be a single lumped axle. To start with, the left and right wheels of the same axle are also considered to be single lumped wheels, like a single-track model presented by Jacobson (2021, p. 352). This results in the free-body diagrams shown in Figure 1. Refer to the Appendix: Vehicle Parameters for a comprehensive list of parameters used.

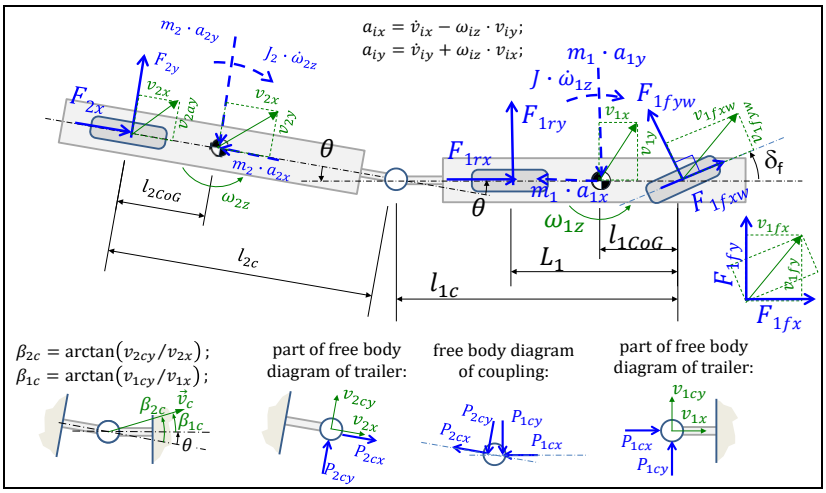


**Figure 1: Free-body diagrams of the single-track model for the articulated heavy vehicles, adapted from Jacobson (2021, p. 352)**

Equations resulting from the tractor's force equilibrium in the longitudinal and lateral directions, and yaw moment equilibrium around its center of gravity are as follows:

$$\begin{cases} m_1 \cdot (\dot{v}_{1x} - \omega_{1z} \cdot v_{1y}) = F_{1fx} + F_{1rx} + P_{1x} \\ m_1 \cdot (\dot{v}_{1y} + \omega_{1z} \cdot v_{1x}) = F_{1fy} + F_{1ry} + P_{1y} \\ J_1 \cdot \dot{\omega}_{1z} = F_{1fy} \cdot l_{1CoG} - F_{1ry} \cdot (L_1 - l_{1CoG}) - P_{1y} \cdot (l_{1c} - l_{1CoG}) \end{cases} \quad \textbf{(1)}$$

The semitrailer has the same set of equilibrium equations given by:

$$\begin{cases} m_2 \cdot (\dot{v}_{2x} - \omega_{2z} \cdot v_{2y}) = F_{2x} + P_{2x} \\ m_2 \cdot (\dot{v}_{2y} + \omega_{2z} \cdot v_{2x}) = F_{2y} + P_{2y} \\ J_2 \cdot \dot{\omega}_{2z} = -F_{2y} \cdot l_{2CoG} + P_{2y} \cdot (l_{2c} - l_{2CoG}) \end{cases} \quad \textbf{(2)}$$

The force equilibrium along the longitudinal and lateral directions for the coupling in between the tractor and the semitrailer are expressed as:

$$\begin{cases} P_{1x} + P_{2x} \cdot \cos\theta + P_{2y} \cdot \sin\theta = 0 \\ P_{1y} - P_{2x} \cdot \sin\theta + P_{2y} \cdot \cos\theta = 0 \end{cases} \quad \textbf{(3)}$$

The compatibility equations for the tractor velocities shown in Figure 1 result in the following set of equations:

$$\begin{cases} v_{1fy} = v_{1y} + \omega_{1z} \cdot l_{1CoG} \\ v_{1ry} = v_{1y} - \omega_{1z} \cdot (L_1 - l_{1CoG}) \\ v_{1cy} = v_{1y} - \omega_{1z} \cdot (l_{1c} - l_{1CoG}) \\ v_{1fxw} = v_{1x} \cdot \cos\delta_f + v_{1fy} \cdot \sin\delta_f \\ v_{1fyw} = -v_{1x} \cdot \sin\delta_f + v_{1fy} \cdot \cos\ \delta_f \end{cases} \quad \textbf{(4)}$$

And the compatibility equations for the semitrailer are given by:

$$\begin{cases} v_{2cy} = v_{2y} + \omega_{2z} \cdot (l_{2c} - l_{2CoG}) \\ v_{2ay} = v_{2y} - \omega_{2z} \cdot l_{2CoG} \end{cases} \quad \textbf{(5)}$$

The longitudinal and lateral velocities of the tractor and semitrailer for the coupling can be expressed as:

$$\begin{cases} v_{1x} = +v_{2x} \cdot \cos\theta + v_{2cy} \cdot \sin\theta \\ v_{1cy} = -v_{2x} \cdot \sin\theta + v_{2cy} \cdot \cos\theta \end{cases} \quad \textbf{(6)}$$

The yaw rate difference of the two units gives the rate of articulation angle as:

$$\dot{\theta} = \omega_{1z} - \omega_{2z} \quad \textbf{(7)}$$

The lateral wheel slips for two units are formulated as:

$$s_{1fy} = \frac{v_{1fyw}}{|v_{1fxw}|} \quad , \quad s_{1ry} = \frac{v_{1ry}}{|v_{1rx}|} \quad , \quad s_{2y} = \frac{v_{2ay}}{|v_{2x}|} \quad \textbf{(8)}$$

The static normal loads of the tractor front axle ($F_{1fz}$), rear axle ($F_{1rz}$) and semitrailer axle ($F_{2z}$) are found with the following equations and are assumed to be constant throughout all the maneuvers, hence longitudinal load transfer is neglected:

$$\begin{cases} F_{1fz} = \dfrac{L_1 - l_{1CoG}}{L_1} \cdot m_1 \cdot g + \dfrac{l_{2CoG}}{l_{2c}} \cdot m_2 \cdot g \cdot \dfrac{L_1 - l_{1c}}{L_1} \\ F_{1rz} = \dfrac{l_{1CoG}}{L_1} \cdot m_1 \cdot g + \dfrac{l_{2CoG}}{l_{2c}} \cdot m_2 \cdot g \cdot \dfrac{l_{1c}}{L_1} \\ F_{2z} = \dfrac{l_{2c} - l_{2CoG}}{l_{2c}} \cdot m_2 \cdot g \end{cases} \quad \textbf{(9)}$$

After obtaining the set of equations from (1) to (9) by considering a single-track model, the rest of the equations will be henceforth obtained with a two-track model adapted from Jacobson's two-track model for passenger car (Jacobson, 2021, p. 363) to cover the effects of lateral load transfer. Furthermore, a more realistic combined slip model (Jacobson, 2021, p. 175) will be introduced for modelling the tires compared to the simpler tire model used by Erdinc et al. (2023a).

At the left-hand side of Figure 2, free-body diagrams of the whole tractor unit, tractor sprung body and tractor axles are shown to obtain the equations describing the roll dynamics. All the tractor mass assumed to be sprung, hence masses of the wheels and axles are neglected.

Lumped axle forces of the single-track model can be expressed in terms of wheel forces of the two-track model as follows:

$$\begin{cases} F_{1fz} = F_{1flz} + F_{1frz} \quad , \quad F_{1fy} = F_{1fly} + F_{1fry} \quad , \quad F_{1fyw} = F_{1flyw} + F_{1fryw} \\ F_{1rz} = F_{1rlz} + F_{1rrz} \quad , \quad F_{1ry} = F_{2fly} + F_{2fry} \end{cases} \quad \textbf{(10)}$$

Right and left wheel forces in the vehicle coordinate system can be formulated in the wheel coordinate system as follows:

$$\begin{cases} F_{1flxw} = F_{1flx} \cdot cos\,\delta_f + F_{1fly} \cdot sin\,\delta_f \;,\; F_{1frxw} = F_{1frx} \cdot cos\,\delta_f + F_{1fry} \cdot sin\,\delta_f \\ F_{1flyw} = -F_{1flx} \cdot sin\,\delta_f + F_{1fly} \cdot cos\,\delta_f \;,\; F_{1fryw} = -F_{1frx} \cdot sin\,\delta_f + F_{1fry} \cdot cos\,\delta_f \end{cases} \quad \textbf{(11)}$$

Roll moment equilibrium around center of gravity of the tractor is given by:

$$J_{1sx} \cdot \dot{\omega}_1 = (F_{1flz} + F_{1rlz}) \cdot \frac{w}{2} - (F_{1frz} + F_{1rrz}) \cdot \frac{w}{2} + (F_{1fy} + F_{1ry}) \cdot h_1 + P_{1cy} \cdot (h_1 - h_{1c}) \quad \textbf{(12)}$$

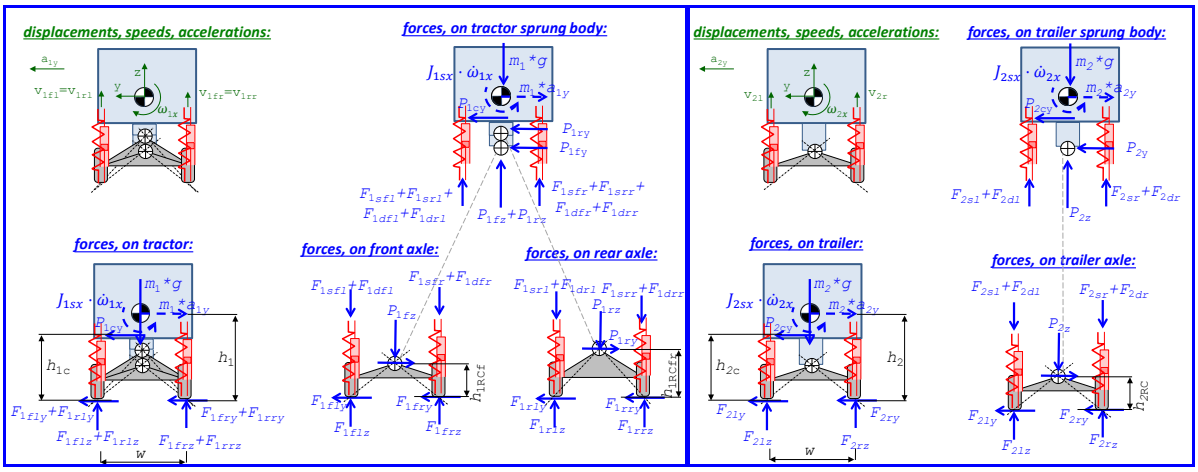


**Figure 2: Free-body diagrams of the tractor and semitrailer to extend the single-track model into two-track model, adapted from Jacobson (2021, p. 363)**

The roll moment equilibrium around the front and rear roll centers of the axles are expressed as:

$$\begin{cases} \left(F_{1flz} - F_{1sfl} - F_{1dfl}\right) \cdot \dfrac{w}{2} - \left(F_{1frz} - F_{1sfr} - F_{1dfr}\right) \cdot \dfrac{w}{2} + F_{1fy} \cdot h_{1RCf} = 0 \\ \left(F_{1rlz} - F_{1srl} - F_{1drl}\right) \cdot \dfrac{w}{2} - \left(F_{1rrz} - F_{1srr} - F_{1drr}\right) \cdot \dfrac{w}{2} + F_{1ry} \cdot h_{1RCr} = 0 \end{cases} \quad \textbf{(13)}$$

At the right-hand side of Figure 2, free-body diagrams of the whole semitrailer unit, semitrailer sprung body and semitrailer axle are shown to obtain the equations describing the roll dynamics. All the semitrailer mass assumed to be sprung, hence masses of the wheels and axles are neglected.

Both units are modelled as fully rigid bodies, hence chassis of both units are assumed to be stiff in the roll direction. Furthermore, coupling is assumed to be roll-free, meaning that units can have different roll angles and there is no roll-moment in the coupling.

Lumped axle forces of the single-track model can be expressed in terms of the wheel forces of the two-track model with the following set of equations:

$$F_{2z} = F_{2lz} + F_{2rz} \quad , \quad F_{2y} = F_{2ly} + F_{2ry} \quad \textbf{(14)}$$

The roll moment equilibrium around center of gravity of the semitrailer is expressed as:

$$J_{2sx} \cdot \dot{\omega}_2 = F_{2lz} \cdot \frac{w}{2} - F_{2rz} \cdot \frac{w}{2} + F_{2y} \cdot h_2 + P_{2cy} \cdot (h_2 - h_{2c}) \quad \textbf{(15)}$$

The roll moment equilibrium around the semitrailer axle roll center is given by:

$$\left(F_{2lz} - F_{2sl} - F_{2dl}\right) \cdot \frac{w}{2} - \left(F_{2rz} - F_{2sr} - F_{2dr}\right) \cdot \frac{w}{2} + F_{2y} \cdot h_{2RC} = 0 \quad \textbf{(16)}$$

Constitutional equations for all the springs in both units can be formulated as:

$$\begin{cases} \dot{F}_{1sfl} = -k_{1sfl} \cdot v_{1fl} \quad , \quad \dot{F}_{1sfr} = -k_{1sfr} \cdot v_{1fr} \\ \dot{F}_{1srl} = -k_{1srl} \cdot v_{1rl} \quad , \quad \dot{F}_{1srr} = -k_{1srr} \cdot v_{1rr} \\ \dot{F}_{2sl} = -k_{2sl} \cdot v_{2l} \quad , \quad \dot{F}_{2sr} = -k_{2sr} \cdot v_{2r} \end{cases} \quad \textbf{(17)}$$

Similarly, constitutional equations for all the dampers in both units can be formulated as:

$$\begin{cases} F_{1dfl} = -d_{1dfl} \cdot v_{1fl} & , \quad F_{1dfr} = -d_{1dfr} \cdot v_{1fr} \\ F_{1drl} = -d_{1drl} \cdot v_{1rl} & , \quad F_{1drr} = -d_{1drr} \cdot v_{1rr} \\ F_{2dl} = -d_{2dl} \cdot v_{2l} & , \quad F_{2dr} = -d_{2dr} \cdot v_{2r} \end{cases} \tag{18}$$

And compatibility equations for the suspension velocities are expressed as:

$$\begin{cases} v_{1fl} = +w \cdot \omega_{1x}/2 & , \quad v_{1fr} = -w \cdot \omega_{1x}/2 \\ v_{1rl} = +w \cdot \omega_{1x}/2 & , \quad v_{1rr} = -w \cdot \omega_{1x}/2 \\ v_{2l} = +w \cdot \omega_{2x}/2 & , \quad v_{2r} = -w \cdot \omega_{2x}/2 \end{cases} \tag{19}$$

Lumped axle longitudinal forces can be formulated in terms of right and left wheel longitudinal forces as:

$$\begin{cases} F_{1fx} = F_{1flx} + F_{1frx} & , \quad F_{1fxw} = F_{1flxw} + F_{1frxw} \\ F_{1rx} = F_{1rlx} + F_{1rrx} & , \quad F_{2x} = F_{2xl} + F_{2xr} \end{cases} \tag{20}$$

Lateral tire forces can be obtained with a friction circle inspired combined slip model as (Jacobson, 2021, p. 175; Svendenius, 2003):

$$\begin{cases} F_{1flyw} = -\mu \cdot F_{1flz} \cdot tanh\left(\frac{C_{1f} \cdot s_{1fy}}{\mu}\right)\sqrt{1 - \left(\frac{F_{1flxw}}{\mu \cdot F_{1flz}}\right)^2} \\ F_{1fryw} = -\mu \cdot F_{1frz} \cdot tanh\left(\frac{C_{1f} \cdot s_{1fy}}{\mu}\right)\sqrt{1 - \left(\frac{F_{1frxw}}{\mu \cdot F_{1frz}}\right)^2} \\ F_{1rly} = -\mu \cdot F_{1rlz} \cdot tanh\left(\frac{C_{1r} \cdot s_{1ry}}{\mu}\right)\sqrt{1 - \left(\frac{F_{1rlx}}{\mu \cdot F_{1rlz}}\right)^2} \\ F_{1rry} = -\mu \cdot F_{1rrz} \cdot tanh\left(\frac{C_{1r} \cdot s_{1ry}}{\mu}\right)\sqrt{1 - \left(\frac{F_{1rrx}}{\mu \cdot F_{1rrz}}\right)^2} \\ F_{2ly} = -\mu \cdot F_{2lz} \cdot tanh\left(\frac{C_{2} \cdot s_{2y}}{\mu}\right)\sqrt{1 - \left(\frac{F_{2lx}}{\mu \cdot F_{2lz}}\right)^2} \\ F_{2ry} = -\mu \cdot F_{2rz} \cdot tanh\left(\frac{C_{2} \cdot s_{2y}}{\mu}\right)\sqrt{1 - \left(\frac{F_{2rx}}{\mu \cdot F_{2rz}}\right)^2} \end{cases} \tag{21}$$

This tire model includes combined slip due to the square root terms. These terms result in decreases in the lateral forces (both the effective cornering stiffness, and maximum lateral force) when longitudinal forces (due to propulsion or braking) exist. This model is more accurate when the wheel forces are close to the saturation, and less accurate for smaller forces as Jacobson (2021) and Svendenius (2003) discuss. However, as the usage of this model in this paper is to study the yaw instabilities, the tire forces are expected to be saturated during the yaw instabilities, where the model is more accurate. The advantage of this formulation is being able to scale down the lateral force as a function of longitudinal force like well-known combined slip formulations (where the vectoral sum of the longitudinal and lateral slips are used), but without involving the longitudinal slip. Furthermore, hyperbolic tangent formulation is a simple, yet good approximation for the lateral force and lateral slip relationship (Jacobson, 2021, p. 136; Metzler et al., 2021). For the small lateral slip values, lateral force increases in a linear form with constant cornering stiffness. For the higher lateral slip values, this linearity is no longer valid and lateral force converges to its maximum value with respect to friction circle model.

The set of equations from (1) to (21) consists of 68 equations and 68 unknowns: $v_{1x}, v_{1y}, \omega_{1z}, v_{2x}, v_{2y}, \omega_{2z}, \theta, F_{1flyw}, F_{1rly}, F_{2\mathrm{ly}}, F_{1fryw}, F_{1rry}, F_{2\mathrm{ry}}, s_{1fy}, s_{1ry}, s_{2y}, P_{1\mathrm{cx}}, P_{1\mathrm{cy}}, P_{2\mathrm{cx}},$

$P_{2cy}, v_{1fxw}, v_{1fyw}, v_{1fy}, v_{1ry}, v_{2ay}, v_{1cy}, v_{2cy}, \omega_{1x}, \omega_{2x}, F_{1fly}, F_{1fry}, F_{1fxw}, F_{1fx}, F_{1rx}, F_{2x}, F_{1yw}, F_{1fy}, F_{1ry}, F_{2y}, F_{1flx}, F_{1frx}, F_{1flz}, F_{1frz}, F_{1rlz}, F_{1rrz}, F_{2lz}, F_{2rz}, F_{1fz}, F_{1rz}, F_{2z}, v_{1fl}, v_{1fr}, v_{1rl}, v_{1rr}, v_{2l}, v_{2r}, F_{1dfl}, F_{1dfr}, F_{1drl}, F_{1drr}, F_{2dl}, F_{2dr}, F_{1sfl}, F_{1sfr}, F_{1srl}, F_{1srr}, F_{2sl}, F_{2sr}.$

The inputs chosen are the longitudinal wheel forces and the steering angle: $[\delta_f, F_{1flxw}, F_{1rlx}, F_{2lx}, F_{1frxw}, F_{1rrx}, F_{2rx}]$.

Comparison of the lateral load transfer between the two-track model and the high-fidelity VTM model confirms that, for quasi-steady-state maneuvers with high lateral acceleration, the load transferred from the inner wheel to the outer wheel is of comparable magnitude.

Volvo Transport Model (VTM) is a high-fidelity model developed by Volvo Group Trucks Technology. It has a multi-body vehicle model, in which every vehicle unit (tractor and semitrailer) is modelled with front and rear chassis rigid bodies (connected with torsional spring and damper to each other), suspended cab rigid body (when applicable), suspended axle rigid bodies, wheel inertias (Fröjd, 2021), PAC2002 semi-empirical tire model (Pacejka, 2005). It is developed with MATLAB®, Simulink®, SimspaceTM MultibodyTM and used for truck controller development, conceptual handling studies, driving simulators, crash reconstructions and functional safety analysis. VTM library is proven to be sufficiently accurate for simulation dynamics of heavy vehicles and it is validated with real tests (Sundström et al., 2012).

## 3. Obtaining the Safe Operating Envelope

The two-track model described in the previous section is used for simulations, which were conducted using the Modelica tool (Modelica, 2023).

To calculate the steering angle, the following formulation is used:

$$\delta_f = L_1/R \tag{22}$$

where the turning radius, $R$, is selected as 72 m. Throughout all simulations, the steering angle is kept constant, meaning that the driver is not counter steering to correct any yaw instability issues. Friction coefficient $\mu$ is selected as 0.3 (snow surface). 4 different initial speeds are tested: [30, 35, 40, 45] km/h. For the first 5 seconds of each simulation, no longitudinal force is applied on the wheels so that the combination reaches to a quasi-steady-state situation. The quasi-steady-state lateral accelerations are measured at the center of gravity on the tractor, resulting in values of [0.95, 1.28, 1.66, 2.07] m/s$^2$ for the given initial speeds and steering angle from equation (22). These lateral accelerations can be normalized with respect to $\mu \cdot g$ (0.3·9.81) to get normalized lateral accelerations $c_y$ = [0.323, 0.436, 0.563, 0.704]. A maximum speed of 45 km/h is tested since this speed is the maximum speed that this combination can reach in the given conditions, according to real tests and high-fidelity model tests presented by Erdinc et al. (2023b).

The longitudinal forces on the right and left wheels of the front axle, denoted as $F_{1flxw}$ and $F_{1frxw}$, respectively, are both set as 0. Hence, a 4x2 electric tractor with no front axle propulsion is considered. As the intention is to study the regenerative braking, only rear axle of the tractor will be braked. Furthermore, to study the regenerative braking with electric trailer, semitrailer axle will also be braked. These 2 axles are braked at the 5$^{th}$ second with a step input (with 0 initial forces) as:

$$\begin{cases} F_{1flxw} = 0 & , \quad F_{1frxw} = 0 \\ F_{1rlx} = c_{tractor} \cdot \mu \cdot \dfrac{F_{1rz}}{2} & , \quad F_{1rrx} = c_{tractor} \cdot \mu \cdot \dfrac{F_{1rz}}{2} \\ F_{2lx} = c_{trailer} \cdot \mu \cdot \dfrac{F_{1rz}}{2} & , \quad F_{2rx} = c_{trailer} \cdot \mu \cdot \dfrac{F_{1rz}}{2} \end{cases} \tag{23}$$

$c_{tractor}$ and $c_{trailer}$, the friction utilizations for the tractor drive axle and semitrailer axle, are selected to vary from 0 to -1 in the steps of 0.01 for braking. Hence, 101 distinct values tested for each. Considering 4 different initial speeds and 101 different friction utilizations for the tractor and semitrailer, a total of 4×101×101 = 40804 simulations are performed. Simulations are terminated either if the tractor reaches to zero velocity due to braking, or if the articulation angle reaches to ±90° which means that a severe jackknifing or trailer swing occurred.

Safety assessment criteria used for detecting unstable maneuvers are expressed by Erdinc et al. (2023a) as:

$$\max(\Delta\beta_{1r}) < 5° \;\; \& \;\; \max(\Delta\beta_{2}) < 3° \tag{24}$$

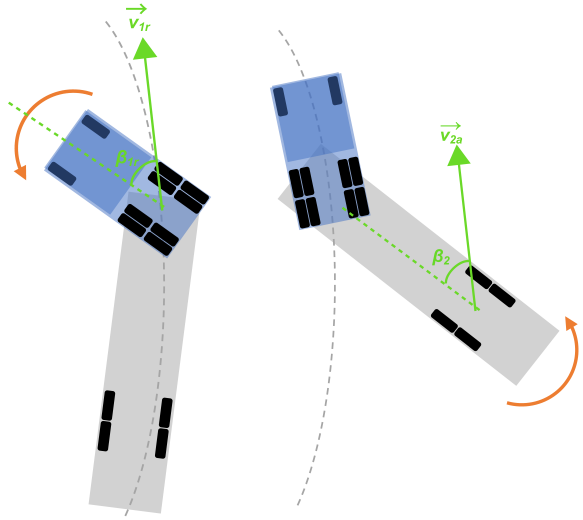


**(a)** **(b)**

**Figure 3: Illustrations of jackknifing (a) and trailer swing (b) for a tractor (blue) and semitrailer (gray)**

which means, the maximum deviation for the side slip angle of the tractor drive axle, $\beta_{1r}$ (shown in Figure 3a), from its quasi-steady-state value (measured just before starting to brake) should be less than 5°. Similarly, the maximum deviation for the side slip angle of the semitrailer axle, $\beta_2$ (shown in Figure 3b), from its quasi-steady-state value should be less than 3°. The maneuver is deemed as unsafe if any of these criteria are not met. Otherwise, it will be considered as safe. Figure 4 shows the SOEs obtained for four different speeds using the VTM model (with no slip controller). The SOEs are represented as background colors, with green indicating safe maneuvers and red indicating unsafe maneuvers according to equation (24). The SOEs obtained using the single-track model presented by Erdinc et al. (2023a) are shown with yellow lines. Additionally, the SOEs obtained using the two-track model presented in this paper are shown as blue lines. The simulated vehicle combinations are same in all 3 models, and its parameters for the two-track model are given in Appendix: Vehicle Parameters.

It has been shown that the SOE obtained with single-track model is not matching with the SOE obtained with high-fidelity model, especially for the high lateral accelerations. On the other hand, the SOE obtained with two-track model is quite close to the SOE obtained with high-fidelity model, except for the upper parts of the last 2 plots for higher lateral accelerations. These upper red areas are where the trailer swing occurs. The right parts of each plot, on the other hand, showing a good match for the SOEs obtained with high-fidelity model and the two-track model. Note that, the SOE obtained with high-fidelity model (shown with red and green) has less data points (11×11 for each plot, unlike 101×101 for single-track and two-track models), hence, resolution is less. But still both high-fidelity model and two-track model

envelopes are in good agreement also on the right-hand sides of the envelopes, which defines where the jackknifing occurs.

From all the graphs, it is evident that the trailer swing area (located on the top) is not significantly influenced by the amount of braking applied to the tractor ($c_{tractor}$). Therefore, the upper boundary of the graph appears almost parallel to the x-axis.

On the other hand, the right boundary, which determines the point of jackknifing, is not parallel to the y-axis and has a positive slope. This suggests that if the semitrailer is also braked, the tractor can be braked further without causing jackknifing. In such situations, stretch braking and applying more tension force on the coupling can help to maintain yaw stability.

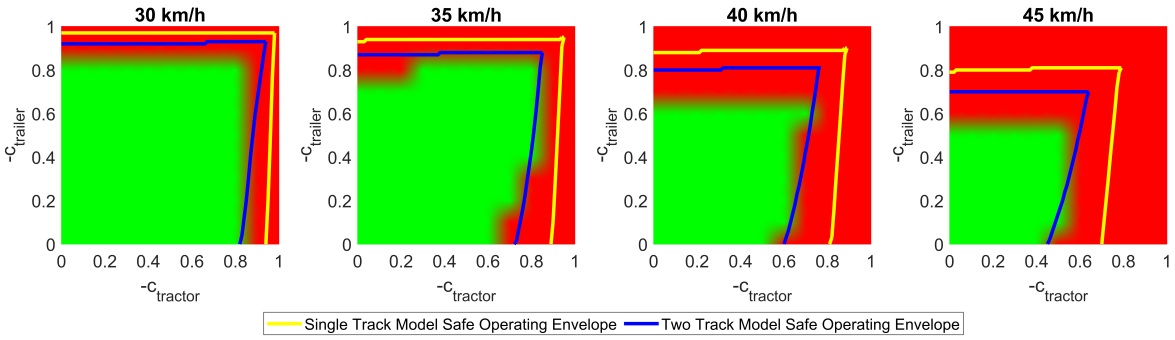


**Figure 4: SOE obtained with single track model (yellow line), two-track model (blue line) and high-fidelity VTM model without slip controller (red/green background)**

The high-fidelity model used to create the SOE shown in Figure 4 has no slip controller, hence the comparison of the single-track and two-track models are fair comparisons. In Figure 5, on the other hand, very same SOEs obtained with the single-track and two-track models are shown, together with the VTM high-fidelity model, but with slip controller. This SOE and the model are validated with real tests by Erdinc et al. (2023b) and shown that they are accurate and safe. The slip controller, in this case, keeps the longitudinal slips lower than 10%. This leads to have more lateral force capability and eventually improves yaw stability. Hence, the SOE is bigger in this case, compared to the one shown in Figure 4.

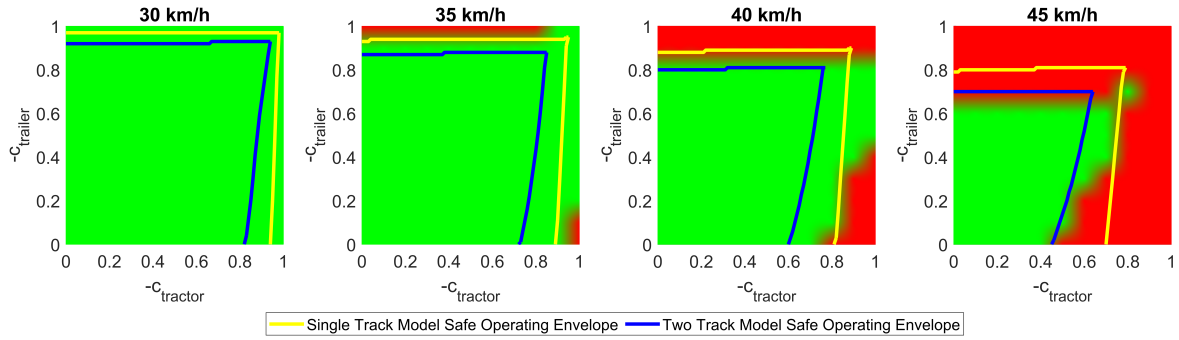


**Figure 5: SOE obtained with single track model (yellow line), two-track model (blue line) and high-fidelity VTM model with slip controller (red/green background)**

Even though the SOE obtained with the two-track model is bigger (for the trailer swing area) than the SOE obtained with the VTM for the high lateral accelerations at the last 2 plots in Figure 4, this pattern does not hold in Figure 5. The SOE obtained with the two-track model lies inside the SOE obtained with the high-fidelity model in Figure 5 for all lateral accelerations.

Hence, when the force distribution for various units and actuators is based on the SOE obtained from the two-track model, it ensures that there will be no yaw instability. This is because the slip controller becomes activated once the longitudinal slips start to increase, thereby preserving sufficient lateral force capability for the tires.

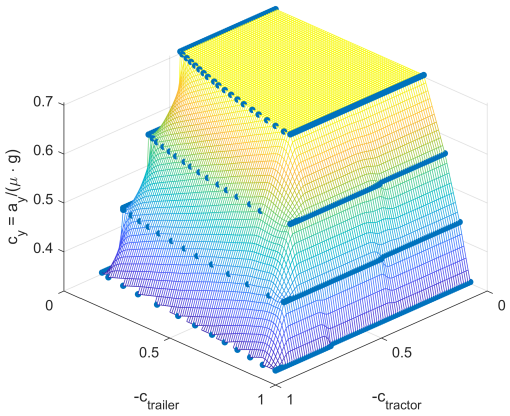


**Figure 6 : 3 dimensional SOE obtained with two-track model**

In Figure 6, a 3-dimensional SOE is shown. This SOE is obtained by using 4 slices of the SOE obtained with the two-track model shown (with blue lines) in Figure 4. 4 slices are stacked along the vertical axis, which represents the normalized lateral acceleration (normalized with respect to the friction coefficient and gravitational constant). 2 other axes represent the friction utilizations with tractor and semitrailer. Only 4 normalized lateral accelerations are simulated, the limits of the SOE are marked with blue dots, for $c_y$ = [0.323, 0.436, 0.563, 0.704], and the intermediate values are interpolated, but denser lateral accelerations can be simulated to obtain a higher resolution envelope along the vertical axis. As the real vehicle and high-fidelity model cannot exceed $c_y$ = 0.704 for the given conditions (Erdinc et al., 2023b), any higher $c_y$ is not simulated and the SOE is limited with maximum normalized lateral acceleration of 0.704, but larger $c_y$ values can anyway be simulated such as done by Erdinc et al. (2023a) and SOE can cover larger $c_y$ values too. This 3-dimensional SOE can be used to limit the control allocation, for example by means of combination of several constraints representing the SOE and the resulting control strategy becomes safe for all lateral accelerations and still solves the control allocation problem as energy efficient as possible. For an electric tractor and conventional semitrailer example, the trivial control allocation strategy for the best energy efficiency would be to use only regenerative braking through the electric motors installed at tractor. However, the proposed SOE will limit the maximum regenerative braking force with certain amount of friction utilization for the given lateral acceleration. The rest of the brake force request, therefore, will be realized by the semitrailer foundation brakes.

## 4. Conclusion

This paper introduces a nonlinear two-track model for investigating the yaw instabilities of tractor and semitrailer combinations. To enhance the model's accuracy for brake-in-turn and propel-in-turn maneuvers, a combined slip model is incorporated. The model also accounts for the combination's roll dynamics, assuming a roll-stiff chassis and roll-free coupling joints. With the given assumptions, lateral load transfer is in the comparable magnitude with the VTM high-fidelity model.

The SOEs obtained with the single-track model (Erdinc et al., 2023a), the two-track model and VTM high-fidelity model (Erdinc et al.,2023b) compared with each other. Two different set of SOEs from the high-fidelity model are considered: with and without the slip controller. The first option is a fair comparison to see the accuracy of the SOEs obtained with simpler models, since the simpler models also don't have slip control. In this comparison, the SOE obtained with the single-track model is found to be larger than the one obtained with VTM, especially for the high lateral accelerations. The main reason is that single-track model lacks the lateral load transfer which becomes significant at high lateral accelerations. Second reason is that the

single-track model used here lacks the combined slip. Although the maximum wheel force is saturated with respect to the friction circle, the cornering stiffness is assumed to be constant up to saturation and is not affected by the presence of longitudinal force or slip.

The two-track model, on the other hand, includes the lateral road transfer and roll degree of freedom. Hence, it is expected to be more accurate at high lateral accelerations. Furthermore, a friction circle inspired combined slip model (Jacobson, 2021, p. 175) together with hyperbolic tangent formulation (Jacobson, 2021, p. 136) is used to model the lateral tire force versus lateral tire slip relationship. The two-track model gives a very similar sized SOE as the high-fidelity model, except the trailer swing area at high lateral accelerations. The reason for this difference can be due to the simplifications and assumptions done in two-track model, such as assuming no unsprung mass, assuming lumped axles for the rear axle group of the tractor and semitrailer axle group (high-fidelity model has a 6x4 tractor and semitrailer with 2 lowered axles while the two-track model assumes the axle groups are lumped into single axles), neglecting the longitudinal load transfer and pitch dynamics, neglecting the roll compliance of the chassis, assuming roll-free coupling.

All simulations are done considering the snow surface with friction coefficient of 0.3, but for higher friction, a larger longitudinal load transfers can be obtained. To address this, the longitudinal load transfer can be incorporated into the two-track model, as well as each individual axle can be modelled instead of assuming lumped axles. Moreover, by modeling the chassis roll compliance and the roll reaction forces at the coupling, the accuracy of the model can be further enhanced. As a result, the fidelity of the two-track model can be increased.

The two-track model is also compared with the VTM model equipped with a slip controller that has been validated in real vehicle tests, as reported by Erdinc et al. (2023b). The inclusion of slip control systems helps to enhance vehicle stability by limiting longitudinal slip, which in turn allows for larger lateral force capabilities. It is observed that the envelope obtained with two-track vehicle model lies inside the envelope obtained with the high-fidelity vehicle model. Hence, although there may be some inaccuracies in the envelope obtained with the two-track model (compared to VTM without slip controller), it still provides a reliable estimate of the vehicle combination's performance. SOE obtained with two-track model is sufficiently conservative and safe combinations of tractor and semitrailer actuator forces obtained with it are shown to be safe in high fidelity simulations with more realistic slip control.

Erdinc et al. (2023a, 2023b) showed that SOE obtained for propulsion is not exactly same with the SOE obtained for braking. Although not studied in this paper, SOEs for propulsion strategies can be obtained with the non-linear two-track model and with the similar methodology explained in Section 3.

By simulating a wide range of scenarios that incorporate different vehicle and environmental parameters (such as friction, speed, turning radius, and load distribution), a comprehensive set of SOEs for each condition can be generated. These SOEs can then be stored in the electronic control units of vehicles, where they can be utilized to limit control allocation and enhance overall safety during driving.

The two-track model presented in this paper has been demonstrated to accurately handle high lateral accelerations, making it an effective tool for studying yaw instabilities. It can be used with a simple driver model for motion prediction to simulate a short time horizon and predict any upcoming yaw instability. By doing so, preventative actions can be taken, such as adjusting speed or changing force allocation between vehicle units to avoid potential safety risks. Thus, the two-track model represents a valuable contribution to enhancing vehicle safety.

## 5. Appendix: Vehicle Parameters

| Parameter | Description | Value | Unit |
|---|---|---|---|
| $m_1$ | Mass of the tractor | 10250 | kg |
| $m_2$ | Mass of the semitrailer | 13500 | kg |
| $J_1$ | Yaw moment of inertia of the tractor | 48758 | kg·m$^2$ |
| $J_2$ | Yaw moment of inertia of the semitrailer | 83913 | kg·m$^2$ |
| $C_{1f}$, $C_{1r}$, $C_2$ | Cornering stiffness of the tractor and semitrailer axles | 6 | - |
| $L_1$ | Tractor wheelbase | 4.085 | m |
| $l_{1c}$ | Distance between coupling to the front axle of tractor | 3.7725 | m |
| $l_{2c}$ | Distance between the coupling to the semitrailer axle | 7.05 | m |
| $l_{1CoG}$ | Distance between the CoG and the front axle of tractor | 1.534 | m |
| $l_{2CoG}$ | Distance between the CoG and the semitrailer axle | 1.9315 | m |
| $k_{1sfl}$, $k_{1sfr}$ | Suspension stiffness coefficients for each tractor front wheel suspension | 232550 | N/m |
| $d_{1dfl}$, $d_{1dfr}$ | Suspension damping coefficients for each tractor front wheel suspension | 7059.5 | N·s/m |
| $k_{1srl}$, $k_{1srr}$ | Suspension stiffness coefficients for each tractor rear wheel suspension | 461300 | N/m |
| $d_{1drl}$, $d_{1drr}$ | Suspension damping coefficients for each tractor rear wheel suspension | 16981 | N·s/m |
| $k_{2sl}$, $k_{2sr}$ | Suspension stiffness coefficients for each semitrailer wheel suspension | 1500000 | N/m |
| $d_{2dl}$, $d_{2dr}$ | Suspension damping coefficients for each semitrailer wheel suspension | 30000 | N·s/m |
| $h_1$ | CoG height of the tractor | 0.92 | m |
| $h_2$ | CoG height of the semitrailer | 0.92 | m |
| $h_{1RCf}$ | Roll center height of the tractor front axle | 0.413 | m |
| $h_{1RCr}$ | Roll center height of the tractor rear axle | 0.83 | m |
| $h_{2RC}$ | Roll center height of the semitrailer axle | 0.52 | m |
| $h_{1c}$, $h_{2c}$ | Coupling height | 1.013 | m |
| $J_{1sx}$ | Roll moment of inertia of the tractor (sprung) | 4914.8 | kg·m$^2$ |
| $J_{2sx}$ | Roll moment of inertia of the semitrailer (sprung) | 4357.7 | kg·m$^2$ |
| $w$ | Track width | 2 | m |
| $c_{tractor}$ | Tractor drive axle's friction utilization | [-1, 0] | - |
| $c_{trailer}$ | Semitrailer axle's friction utilization | [-1, 0] | - |

## 6. References


- Beal C, Bobier C, Gerdes J. Controlling vehicle instability through stable handling envelopes. In: Proceedings of the ASME 2011 Dynamic Systems and Control Conference and Bath/ASME Symposium on Fluid Power and Motion Control; 2011 Oct 31-Nov 2; Arlington, VA. ASME; 2011.
- Bobier CG, Gerdes JC. Envelope control: stabilizing within the limits of handling using a sliding surface. In: IFAC Proceedings Volumes. 6th IFAC Symposium on Advances in Automotive Control; 2010 Jul 12-14; Munich, Germany. vol. 43(7). IFAC; 2010. p. 162–167. Available from: https://www.sciencedirect.com/science/article/pii/S1474667015368233.
- Bobier CG, Gerdes JC. Staying within the nullcline boundary for vehicle envelope control using a sliding surface. Vehicle System Dynamics. 2013;51(2):199–217. Available from: https://doi.org/10.1080/00423114.2012.720377.

- Brown M, Funke J, Erlien S, et al. Safe driving envelopes for path tracking in autonomous vehicles. Control Engineering Practice. 2017;61:307–316. Available from: https://www.sciencedirect.com/science/article/pii/S0967066116300831.
- Cui Q, Ding R, Wei C, et al. Path-tracking and lateral stabilisation for autonomous vehicles by using the steering angle envelope. Vehicle System Dynamics. 2021;59(11):1672–1696. Available from: https://doi.org/10.1080/00423114.2020.1776344.
- Erdinc U, Jonasson M, Kati MS, Jacobson B, Fredriksson J, Laine L. Safe operating envelope based on a single-track model for yaw instability avoidance of articulated heavy vehicles. 2023a. [Unpublished manuscript].
- Erdinc U, Jonasson M, Kati MS, Jacobson B, Fredriksson J, Laine L. 2023b. Validation of safe operating envelope for articulated heavy vehicles. [Unpublished manuscript].
- Fröjd N. Handling analysis and control development of commercial trucks with Volvo Transport Models. Material presented at: MATLAB EXPO 2021; 2021 May 4-5. Available from: https://se.mathworks.com/videos/handling-analysis-and-control-development-of-commercial-trucks-with-volvo-transport-models-1622035211192.html.
- Hansson A, Andersson E, Laine L, Kati MS, Erdinc U, Jonasson M. Safe operating envelope for limiting actuation of electric trailer in tractor-semitrailer combination. 2022 IEEE 25th International Conference on Intelligent Transportation Systems (ITSC), 2022, pp. 3886-3893, Available from: https://doi.org/10.1109/ITSC55140.2022.9922094.
- Jacobson B. Vehicle dynamics compendium. Gothenburg (Sweden): Chalmers University of Technology; 2021.
- Janardhanan S, Laine L, Jonasson M, et al. Motion control and power coordination of electric propulsion and braking distributed on multiple axles on heavy vehicles. 2022 IEEE Vehicle Power and Propulsion Conference (VPPC), 2022, pp. 1-8 Available from: https://doi.org/10.1109/VPPC55846.2022.10003450.
- Lombaerts T, Schuet S, Acosta D, et al. On-line safe flight envelope determination for impaired aircraft. In: Bordeneuve-Guibé J, Drouin A, Roos C, editors. Advances in Aerospace Guidance, Navigation and Control: Selected Papers of the Third CEAS Specialist Conference on Guidance, Navigation and Control; 2015 Apr 13-15; Toulouse, France. Springer; 2015. p. 263–282. Available from: https://link.springer.com/content/pdf/10.1007/978-3-319-17518-8.pdf.
- Lombaerts T, Schuet S, Wheeler K, et al. Safe maneuvering envelope estimation based on a physical approach. In: Proceedings of the AIAA Guidance, Navigation, and Control (GNC) Conference; 2013 Aug 19-22; Boston, MA. AIAA; 2013. Available from: https://arc.aiaa.org/doi/abs/10.2514/6.2013-4618.
- Metzler M , Tavernini D , Gruber P et al. On Prediction Model Fidelity in Explicit Nonlinear Model Predictive Vehicle Stability Control. IEEE Transactions on Control Systems Technology. 2020;29(5):1964-1980. Available from: http://dx.doi.org/10.1109/TCST.2020.3012683.
- Modelica.org [Internet]. Munich (Germany): The Modelica Association; [cited 2023 Mar 22]. Available from: https://modelica.org/
- Pacejka HB. Tyre and vehicle dynamics. 2nd ed. Oxford (UK): Butterworth-Heinemann; 2005.
- Park JY, Kim N. Design of a safety operational envelope protection system for a submarine. Ocean Engineering. 2018;148:602–611. Available from: https://www.sciencedirect.com/science/article/pii/S0029801817306832.
- Prime R, McIntyre M, Reeves D. Implementation of an improved safe operating envelope. In: Proceedings of the International Youth Nuclear Congress; 2008 Sep 20-26; Interlaken, Switzerland. IYNC; 2008. p. 408.1–408.7. Available from: https://inis.iaea.org/collection/NCLCollectionStore/_Public/40/048/40048172.pdf.
- Sundström P, Laine L. Validation of VTM model of tractor 4x2 with semitrailer using winter test results from Arjeplog 2011w11 P2685. Gothenburg (SE): Volvo Group Trucks Technology; 2012. (Engineering report; ER-624557).
- Svendenius J. Tire Models for Use in Braking Applications [Licentiate Thesis]. Lund (Sweden): Department of Automatic Control, Lund Institute of Technology (LTH); 2003. Available from: https://portal.research.lu.se/files/4386030/8840416.pdf.
- Van Oort ER, Chu QP, Mulder JA. Maneuver envelope determination through reachability analysis. In: Holzapfel F, Theil S, editors. Advances in Aerospace Guidance, Navigation and Control: Selected Papers of the 1st CEAS Specialist Conference on Guidance, Navigation and Control; 2011 Apr 13-15; Munich, Germany. Springer; 2011. p. 91–102. Available from: https://link.springer.com/content/pdf/10.1007/978-3-642-19817-5.pdf.
- Zhang Y, De Visser C, Chu QP. Online safe flight envelope prediction for damaged aircraft: a database-driven approach. In: Proceedings of the AIAA Modeling and Simulation Technologies Conference; 2016 Aug 19-22; Boston, MA. AIAA; 2016. Available from: https://pure.tudelft.nl/ws/portalfiles/portal/10445072/Ye_postprint_2.pdf.